Molecular Cell, Volume *73*

Supplemental Information

Promoter Distortion and Opening in the RNA Polymerase II Cleft

Christian Dienemann, Björn Schwalb, Sandra Schilbach, and Patrick Cramer

Figure S1

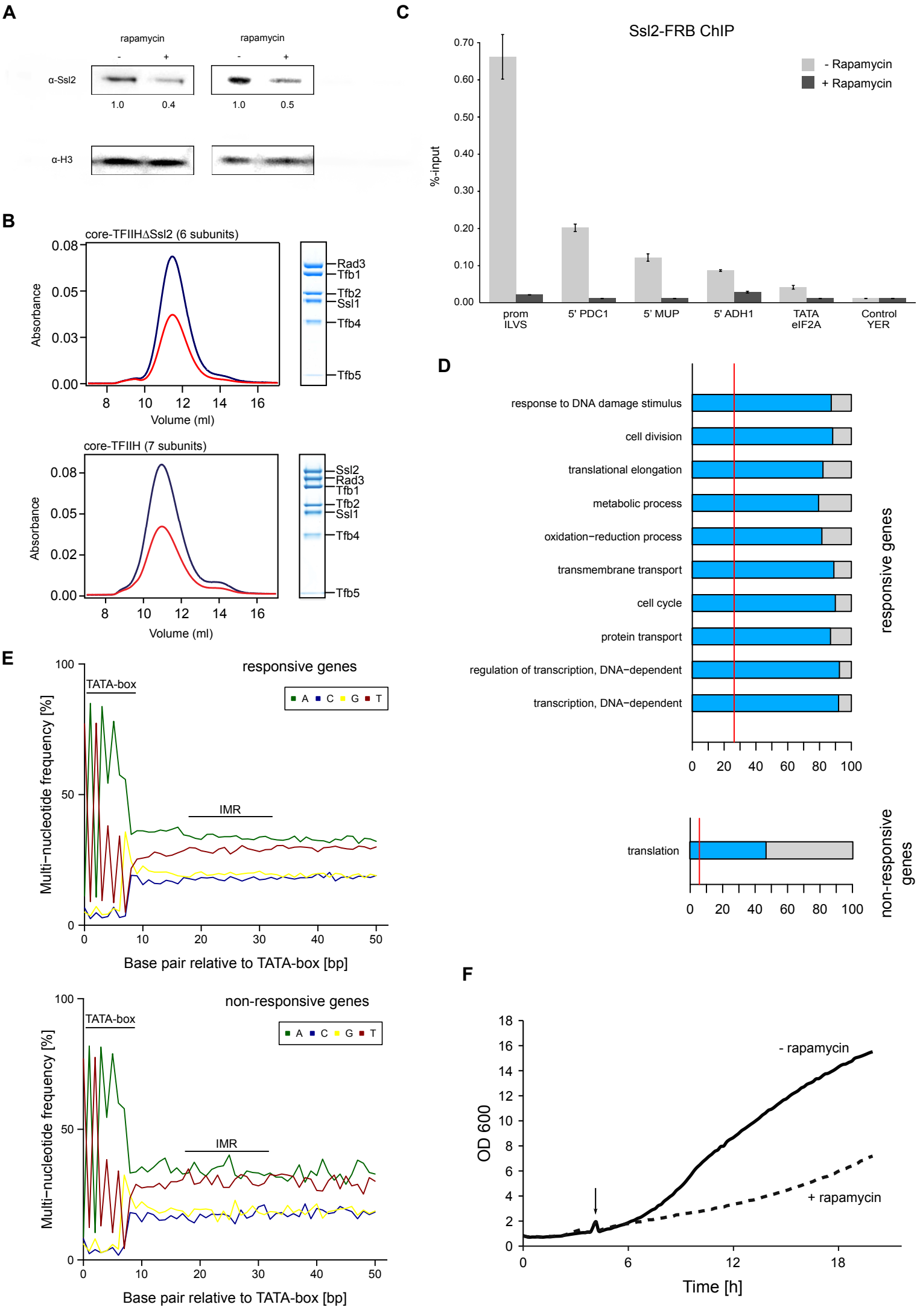
A
rapamycin
rapamycin
α-Ssl2
1.0
0.4
1.0
0.5
α-H3
B
core-TFIIHΔSsl2 (6 subunits)
Absorbance
Volume (ml)
Rad3
Tfb1
Tfb2
Ssl1
Tfb4
Tfb5
core-TFIIH (7 subunits)
Ssl2
Rad3
Tfb1
Tfb2
Ssl1
Tfb4
Tfb5
C
Ssl2-FRB ChIP
- Rapamycin
+ Rapamycin
%-input
prom ILVS
5' PDC1
5' MUP
5' ADH1
TATA eIF2A
Control YER
D
response to DNA damage stimulus
cell division
translational elongation
metabolic process
oxidation−reduction process
transmembrane transport
cell cycle
protein transport
regulation of transcription, DNA−dependent
transcription, DNA−dependent
responsive genes
translation
non-responsive genes
E
responsive genes
TATA-box
IMR
Multi−nucleotide frequency [%]
Base pair relative to TATA-box [bp]
non-responsive genes
F
- rapamycin
+ rapamycin
OD 600
Time [h]

Figure S2

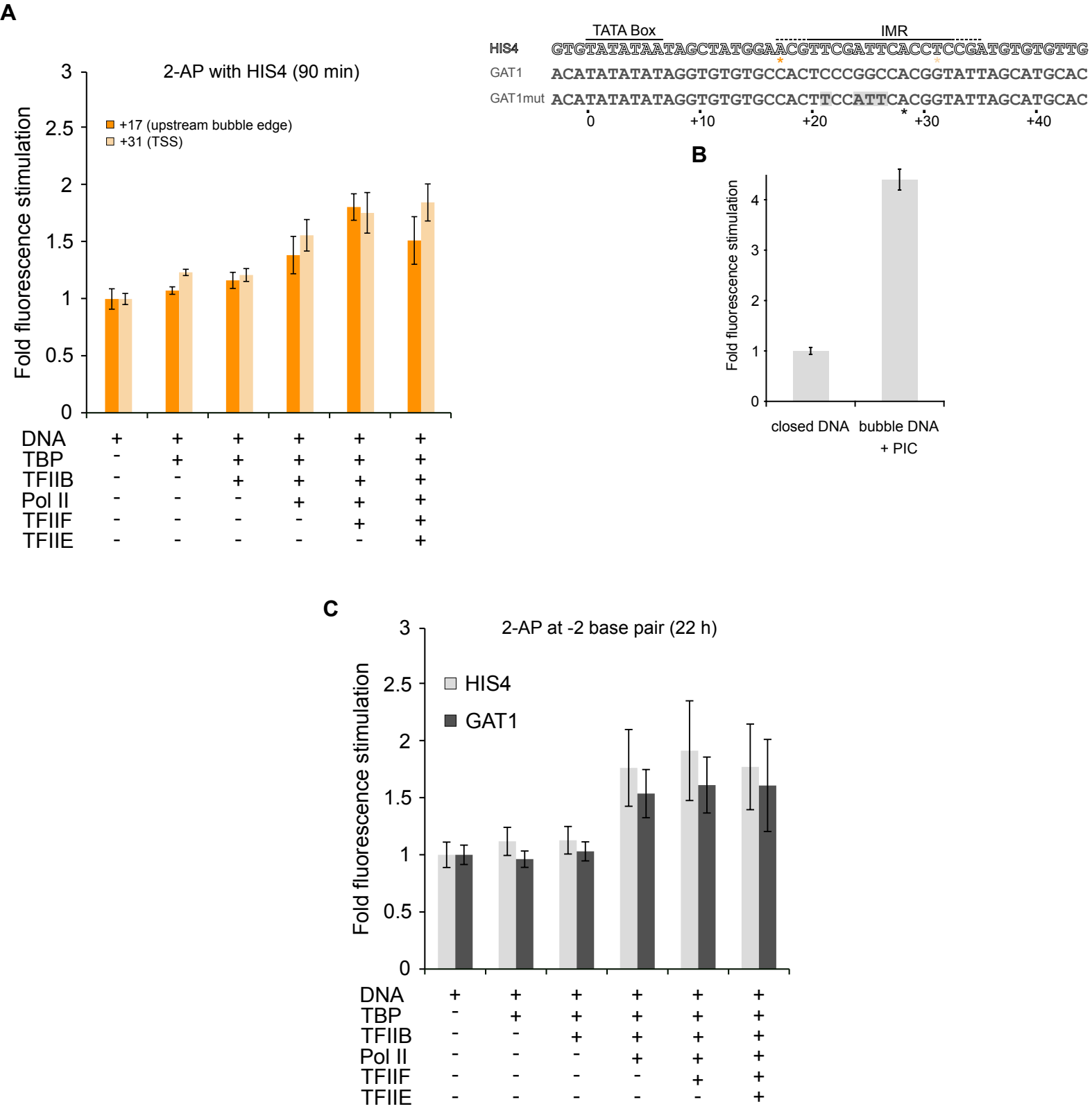
A
2-AP with HIS4 (90 min)
+17 (upstream bubble edge)
+31 (TSS)
Fold fluorescence stimulation
DNA
TBP
TFIIB
Pol II
TFIIF
TFIIE
TATA Box
IMR
HIS4 GTGTATATAAATAGCTATGGAACGTTCGATTCACCTCCGATGTGTGTTG
GAT1 ACATATATATAGGTGTGTGCCACTCCCGGCCACGGTATTAGCATGCAC
GAT1mut ACATATATATAGGTGTGTGCCACTTCCATTCACGGTATTAGCATGCAC
0
+10
+20
+30
+40
B
Fold fluorescence stimulation
closed DNA
bubble DNA
+ PIC
C
2-AP at -2 base pair (22 h)
HIS4
GAT1
Fold fluorescence stimulation
DNA
TBP
TFIIB
Pol II
TFIIF
TFIIE

Figure S3

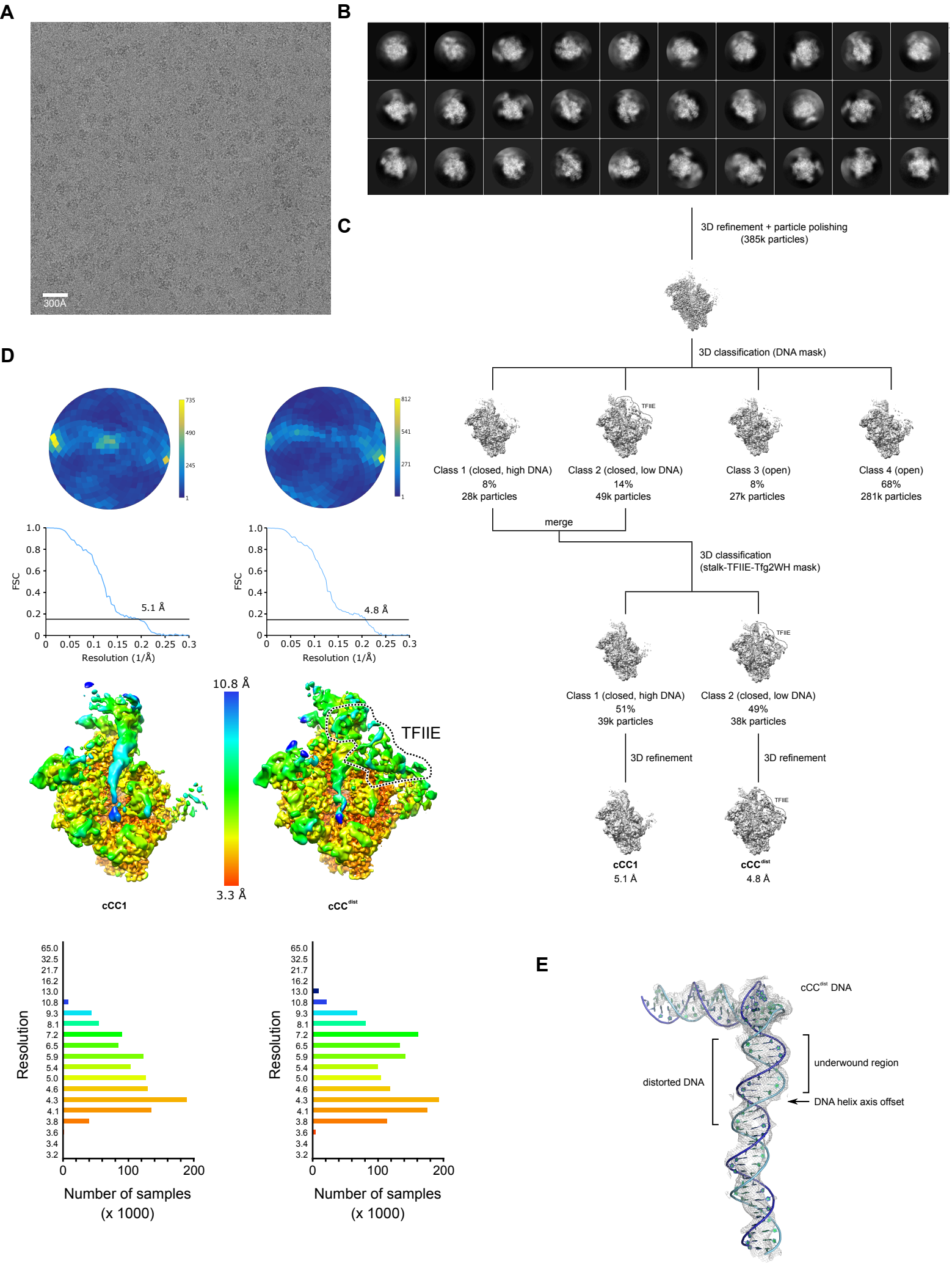
A
300Å
B
C
3D refinement + particle polishing
(385k particles)
3D classification (DNA mask)
TFIIE
Class 1 (closed, high DNA)
8%
28k particles
Class 2 (closed, low DNA)
14%
49k particles
Class 3 (open)
8%
27k particles
Class 4 (open)
68%
281k particles
merge
3D classification
(stalk-TFIIE-Tfg2WH mask)
Class 1 (closed, high DNA)
51%
39k particles
Class 2 (closed, low DNA)
49%
38k particles
3D refinement
3D refinement
cCC1
5.1 Å
cCC^dist
4.8 Å
D
735
490
245
1
812
541
271
1
FSC
5.1 Å
4.8 Å
Resolution (1/Å)
10.8 Å
3.3 Å
TFIIE
cCC1
cCC^dist
Resolution
Number of samples
(x 1000)
E
cCC^dist DNA
distorted DNA
underwound region
DNA helix axis offset

Figure S4

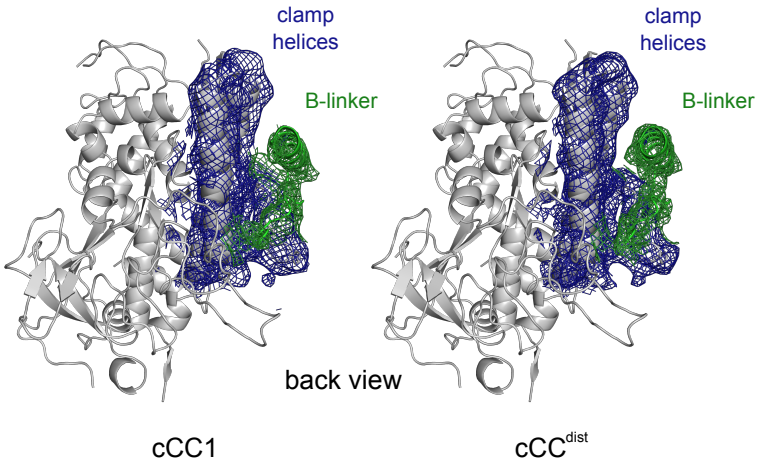

cCC1 cCC^{dist}

Figure S5

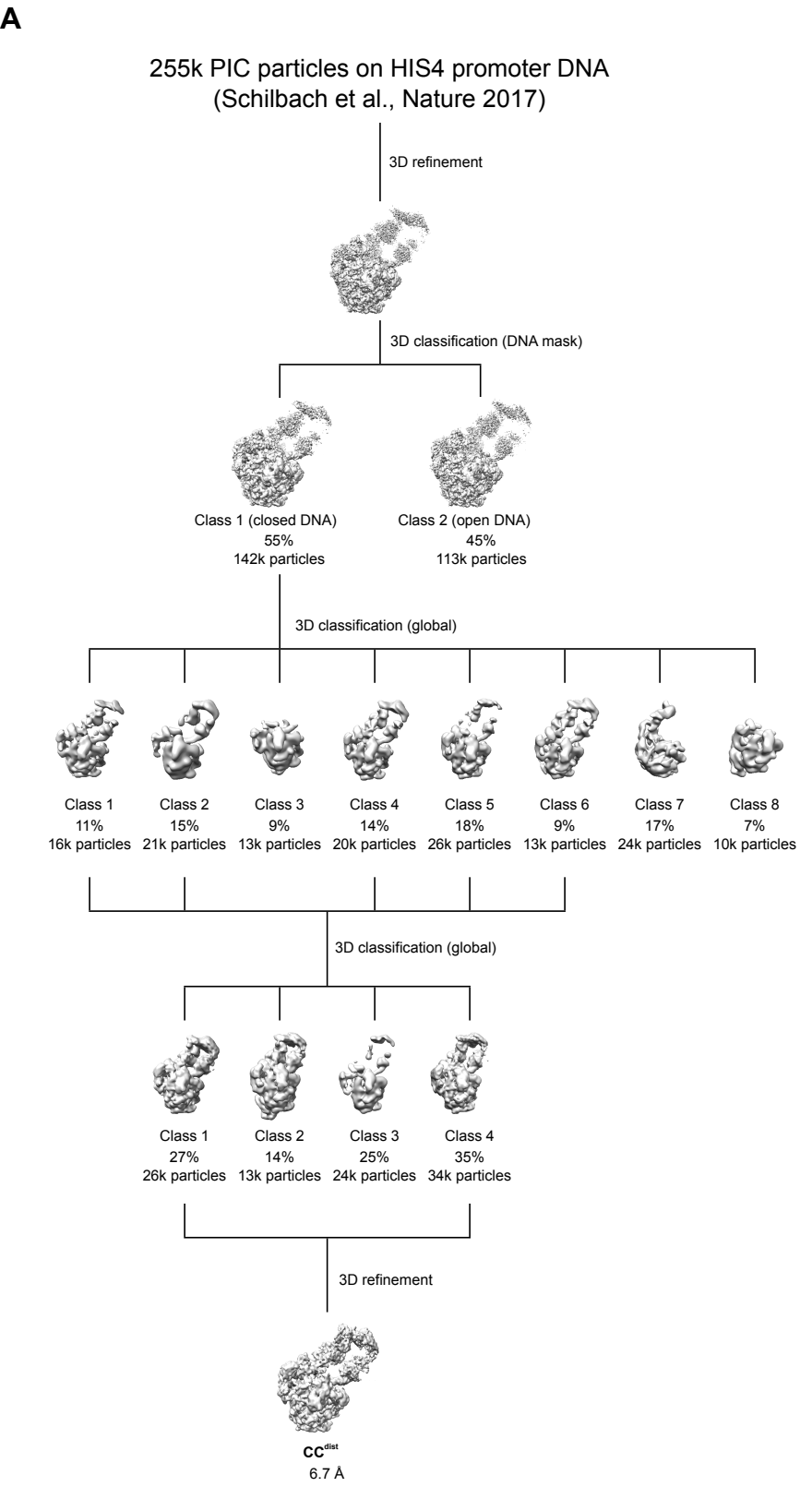
A
255k PIC particles on HIS4 promoter DNA
(Schilbach et al., Nature 2017)
3D refinement
3D classification (DNA mask)
Class 1 (closed DNA)
55%
142k particles
Class 2 (open DNA)
45%
113k particles
3D classification (global)
Class 1
11%
16k particles
Class 2
15%
21k particles
Class 3
9%
13k particles
Class 4
14%
20k particles
Class 5
18%
26k particles
Class 6
9%
13k particles
Class 7
17%
24k particles
Class 8
7%
10k particles
3D classification (global)
Class 1
27%
26k particles
Class 2
14%
13k particles
Class 3
25%
24k particles
Class 4
35%
34k particles
3D refinement
CC dist
6.7 Å

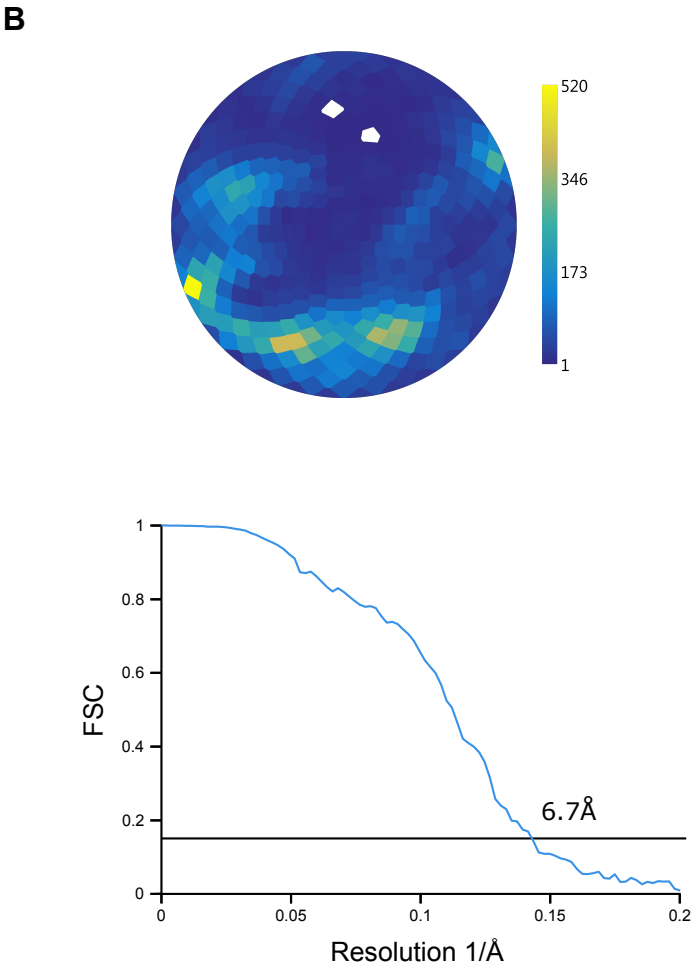
B
520
346
173
1
FSC
1
0.8
0.6
0.4
0.2
0
6.7Å
0
0.05
0.1
0.15
0.2
Resolution 1/Å

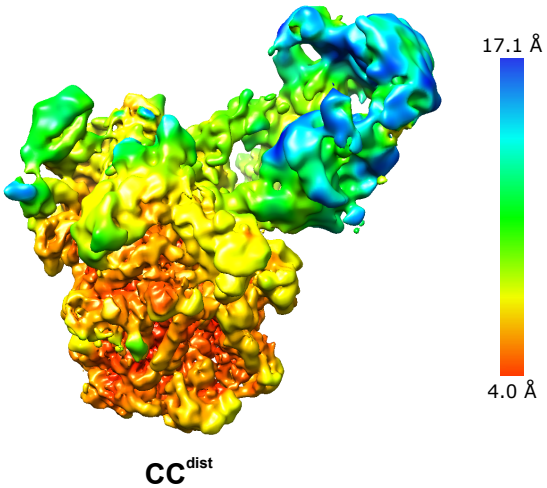
17.1 Å
4.0 Å
CC dist

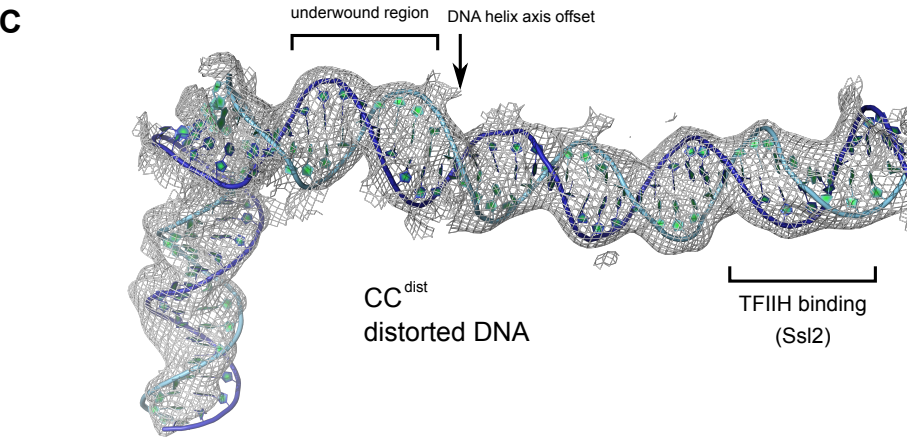
C
underwound region
DNA helix axis offset
CC dist
distorted DNA
TFIIH binding
(Ssl2)

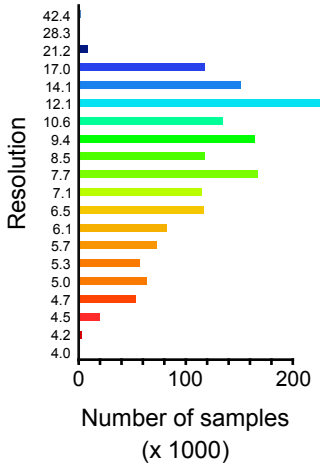
Resolution
42.4
28.3
21.2
17.0
14.1
12.1
10.6
9.4
8.5
7.7
7.1
6.5
6.1
5.7
5.3
5.0
4.7
4.5
4.2
4.0
0
100
200
Number of samples
(x 1000)

Figure S1 | Validations and controls for Ssl2 anchor away, Related to Figure 1

(**A**) Western blot analysis of purified yeast nuclei with and without rapamycin treatment. Ssl2-depletion was detected by specific antibodies. H3 was used as loading control. Two replicates are shown. Quantification shows the factor of band intensity reduction.
(**B**) Yeast TFIIH can be purified without Ssl2. Chromatograms of analytical gel filtrations are shown for wilt type TFIIH and TFIIH lacking the Ssl2 subunit. The integrity of both complexes was detected by SDS-PAGE.
(**C**) Ssl2-FRB ChIP qPCR without and with rapamycin treatment. Genes were chosed from Ssl2-independent (PDC1) and Ssl2-dependent genes (others). Primers for qPCR were chosen in the 5' region of the respective gene close to the promoter. YER is the random chromatin control.
(**D**) GO-term enrichment of Ssl2-dependent and independent genes. Enrichment analysis was done using fisher tests. Top GO categories are sorted by p-values. The blue bars depict the percent fraction of genes that are enriched from each GO term. The red line indicates the proportion of each category that is expected by chance.
(**E**) Ssl2-dependent and -independent genes do not show base enrichment in their IMR. Average base content of promoter regions downstream of TATA for Ssl2-dependent genes are shown in % for each base position. Genes were aligned at their TATA box. TATA box and IMR are marked with solid lines.
(**F**) Rapamycin treatment induces growth phenotype in Ssl2 anchor away yeast. The growth curve of the Ssl2 anchor away strain is shown under normal (solid) and Ssl2 depletion (dashed) conditions. Growth curves were collected over 20 hours in YPD medium at 30°C.

Figure S2 | TFIIH independent opening of HIS4 and GAT1 promoter DNA, Related to Figure 2

(**A**) TFIIH independent opening of HIS4 promoter DNA can be detected across the IMR. 2-aminopurine (2-AP) labels were incorporated at the upstream bubble edge (+17 bases from the TATA box) and around the region where the TSS would be optimally placed (+31). Bar plots show the fluorescence increase normalized to the DNA only reaction.
(**B**) 2-AP Fluorescence stimulation with miss-matched HIS4 promoter DNA. The artificial bubble template DNA was created by introducing mismatches in the template DNA strand.
(**C**) The *GAT1* promoter melts spontaneously *in vitro* after 22 hours. Spontaneous melting of the *GAT1* promoter is achieved after incubation time with cPIC components was extended to 22 hours. Bar plots show the fluorescence increase normalized to the DNA only reaction. 2-AP labelled *HIS4* promoter DNA after 22 hours is shown for comparison. Data is shown as mean ± SEM in all panels.

Figure S3 | Data processing of cCC1 and cCC^{dist}, Related to Figure 3

(**A**) A micrograph representative for the collected data is shown. The micrographs have been contrast enhanced for clarity.
(**B**) Selected 2D classes that were used after manual and 2D-classification based particle cleanup. 2D classes are ordered by number of particles in descending order.
(**C**) Schematic for processing strategy of the cCC1/cCC^{dist} dataset. Reconstructions of each processing step are shown as grey surfaces. Particle numbers are rounded. Resolution is

given according to the 0.143 FSC threshold and with a B-factor of -100Å^2.
(**D**) Angular distribution and Fourier-shell correlation (FSC) plots for cCC1 and cCC^{dist} reconstructions. Angular distribution was calculated in 7.5° orientation bins. The 0.143 FSC threshold is marked in FSC lots as solid line. Local resolution was calculates by a combination of local FSC weighting and B-factor sharpening. The resolution histogram represents the number of samples per resolution bin. Locally filtered volumes of the reconstructions for cCC1 and cCC^{dist} are shown in front view (Figure 3A and B).
(**E**) Model and map of the distorted cCC^{dist} DNA. The model is shown in cartoon representation, the locally filtered map as grey mesh.

Figure S4 | Clamp and B-linker of cCC1 and cCC^{dist}, Related to Figure 3

The B-linker is well ordered in cCC1 and cCC^{dist}.The Pol II clamp and B-linker of cCC1 and cCC^{dist} are shown in cartoon representation. The map for clamp helices and B-linker is shown as blue and green mesh, respectively.

Figure S5 | Data processing of CC^{dist}, Related to Figure 5

(**A**) 3D sorting of PIC particles leads to the CC^{dist} reconstruction. A schematic of the 3D sorting strategy for the CC^{dist} reconstruction is shown. Intermediate reconstructions are shown as grey volumes. Particle numbers are rounded. Resolution is given according to the 0.143 FSC threshold and with a B-factor of -100Å^2.
(**B**) Angular distribution and Fourier-shell correlation (FSC) plots for the CC^{dist} reconstruction. Angular distribution was calculated in 7.5° orientation bins. The 0.143 FSC threshold is indicated as solid line. Local resolution was calculates by a combination of local FSC weighting and B-factor sharpening. Locally filtered volume of CC^{dist} is shown in side view (Figure 5A). The resolution histogram represents the number of samples per resolution bin.
(**C**) Model and map of the distorted CC^{dist} DNA. The model is shown in cartoon representation, the locally filtered map as grey mesh.

Table S1 | Eukaryotic closed complex structures

	Pol II						*Pol I**	*Pol III*
State	**cCC**	**cCC1**	**cCC2**	**CC2**	**cCC^{dist}**	**CC^{dist}**	**CC2**	**CC1**
Reference	Plaschka et al., 2016	this study	He et al., 2016	He et al., 2016	this study	this study	Engel et al., 2017	Vorländer et al., 2018
Resolution	7.8 Å	5.1 Å	5.4 Å	7.2 Å	4.8 Å	8.0 Å	modeled	5.5/4.2 Å
DNA distance from active site	72.9 Å	71.5 Å	55.9 Å	55.9 Å	64.3 Å	64.3 Å	44.9 Å	68.4 Å
DNA conformation	canonical	canonical	canonical	canonical	distorted	distorted	canonical	canonical
Clamp	closed	closed	open	open	closed	closed	open	closed
B-linker	weak	+	-	-	+	+		
B-reader	+	+	-	-	+	+		
TFIIE	weak	-	+	+	+	+		
Tfg2WH	weak	-	+	+	+	+		

* based on structural modeling.